

PCCP

Accepted Manuscript



This is an *Accepted Manuscript*, which has been through the Royal Society of Chemistry peer review process and has been accepted for publication.

Accepted Manuscripts are published online shortly after acceptance, before technical editing, formatting and proof reading. Using this free service, authors can make their results available to the community, in citable form, before we publish the edited article. We will replace this *Accepted Manuscript* with the edited and formatted *Advance Article* as soon as it is available.

You can find more information about *Accepted Manuscripts* in the [Information for Authors](#).

Please note that technical editing may introduce minor changes to the text and/or graphics, which may alter content. The journal's standard [Terms & Conditions](#) and the [Ethical guidelines](#) still apply. In no event shall the Royal Society of Chemistry be held responsible for any errors or omissions in this *Accepted Manuscript* or any consequences arising from the use of any information it contains.

Experimental and computational study of solvent effects on one- and two-photon absorption spectra of chlorinated harmines

Dalibor Hřšak,^{a‡} Lotte Holmegaard,^{a‡} Anton S. Poulsen,^a Nanna H. List,^b Jacob Kongsted,^b M. Paula Denofrio,^c Rosa Erra-Balsells,^d Franco M. Cabrerizo,^{*c} Ove Christiansen^{*a} and Peter R. Ogilby^{*a}

Received Xth XXXXXXXXXXXX 20XX, Accepted Xth XXXXXXXXXXXX 20XX

First published on the web Xth XXXXXXXXXXXX 200X

DOI: 10.1039/b000000x

A combined experimental and computational study of solvent effects on one- and two-photon absorption spectra of three chlorinated harmine derivatives is presented. The systems studied were protonated forms of 6-chloroharmine, 8-chloroharmine and 6,8-dichloroharmine in two solvents, acetonitrile and water. For the computations, polarizable embedding density functional and coupled cluster response theory methods were used. The computations were able to model the solvent-dependent experimental data well. These results demonstrate that reasonably sophisticated computational methods can be successfully applied to accurately study linear and nonlinear spectroscopic properties of comparatively large organic molecules in solution.

1 Introduction

Nonlinear spectroscopic processes, particularly two-photon absorption, have been of great interest to the scientific community in recent decades.^{1,2} One practical application of two-photon absorption (TPA) that sets it apart from one-photon absorption (OPA) is the ability to achieve better spatial resolution in microscope-based optical imaging experiments^{3,4} and photo-initiated polymerization reactions.⁵ From a fundamental perspective, TPA makes it possible to investigate electronic transitions and populate excited states that might otherwise be inaccessible via a linear one-photon process.^{6–8} Two-photon excitation of a given molecule can also result in the photosensitized production of singlet molecular oxygen, O₂(a¹Δ_g); a process that can have both fundamental and spatially resolved practical ramifications.⁹

Over the past ~20 years, the fields of two-photon spectroscopy and microscopy have advanced appreciably with

the systematic production of chromophores that have comparatively large two-photon absorption cross sections.^{1,2,10} More recent efforts have focused on experiments to accurately obtain two-photon spectra and quantify absorption cross sections.^{11–13} These efforts extend to studies of protein-encapsulated chromophores used as mechanistic tools in biological systems.^{7,14,15} Experimental studies have been complemented by a variety of approaches to computationally model two-photon parameters.^{14,16–21}

Theoretical and computational chemistry has become a powerful tool for modeling and predicting specific properties of molecular systems. Accurate description of nonlinear optical processes is an especially challenging computational task, but the development of response theory²² has facilitated efficient solutions to this issue; TPA spectra can be computed from the single residue of the quadratic response function.^{22,23} Response theory can be combined with *ab initio* theoretical models like coupled cluster (CC) theory²³ and with time-dependent density functional theory (TDDFT).²⁴

In many cases, it is sufficient to obtain and model properties of isolated molecules in gas phase systems. However, there is also a great need to quantify and understand the effects of a potentially perturbing environment (*e.g.*, a solvent or an encapsulating protein). Although it is a challenging task to experimentally quantify solvent effects on nonlinear optical properties, remarkable progress has been made in this regard over the past 10 years.^{7,15,25–31} Pertinent issues include the solvent effects on processes used to monitor excited state populations (*i.e.* fluorescence efficiency and the efficiency of collecting the emitted light). Nevertheless, much remains to be done to fully explore the ways that solvent perturbations can influence nonlinear optical transitions. In the least, these

† Electronic Supplementary Information (ESI) available: [details of any supplementary information available should be included here]. See DOI: 10.1039/b000000x/

^a Center for Oxygen Microscopy and Imaging, Aarhus University, Lange-landsgade 140, 8000 Aarhus C, Denmark. Tel: +45 5152 6145, +45 8715 5927; E-mail: ove@chem.au.dk, progilby@chem.au.dk

^b Department of Physics, Chemistry and Pharmacy, University of Southern Denmark, Campusvej 55, 5230 Odense M, Denmark.

^c Instituto de Investigaciones Biotecnológicas, Instituto Tecnológico de Chascomús (IIB-INTECH), Universidad Nacional de San Martín (UNSAM), Consejo Nacional de Investigaciones, Científicas y Técnicas (CONICET), Intendente Marino Km 8.2, CC 164 (B7130IWA), Chascomús, Argentina. E-mail: fcabrerizo@intech.gov.ar

^d CIHIDECAR–CONICET, Departamento de Química Orgánica, Facultad de Ciencias Exactas y Naturales, Universidad de Buenos Aires, Ciudad Universitaria, 1428 Buenos Aires, Argentina

‡ These authors contributed equally to this work.

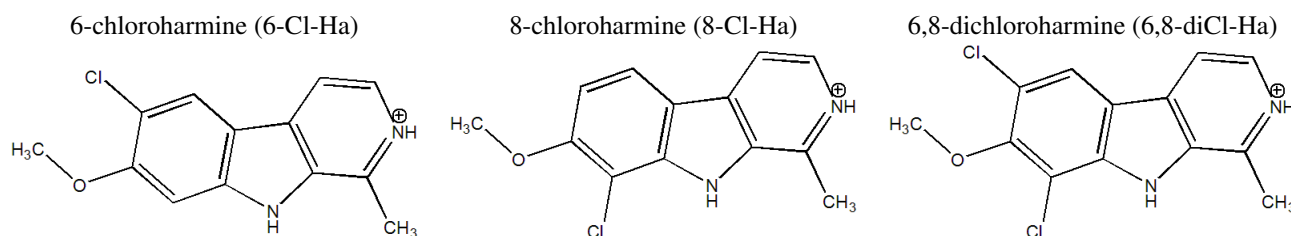


Fig. 1 Protonated chloroharmines selected for experimental and theoretical studies.

have many practical applications given that TPA is used as a tool in a wide range of solvent systems.^{1,2,9,32}

For the present work, we set out to examine solvent effects on one- and two-photon absorption spectra in a combined experimental and computational study. Our goal was to put these phenomena on a more quantitative footing and to gain computational insight into subtle interactions between solute and solvent molecules. One challenge in this regard was to find an appropriate molecular system tractable for both perspectives, and which could still yield useful information. Specifically, from an experimental perspective, we wanted a chromophore that was large enough so that the pertinent transitions occurred at the longer wavelengths most readily accessed with modern fs lasers. From the computational perspective, we wanted a chromophore small enough to readily facilitate high-level computations. Finally, we wanted a system in which the solvents were amenable to both experimental and computational methods used.

To these ends, we settled on the three chlorinated harmines in their protonated form, shown in Figure 1. Harmine and its derivatives are alkaloids belonging to the class of β -carbolines. Although harmines have a number of important photoinitiated properties,^{33,34} key factors for the present study are the spectroscopic features of these molecules. In particular, preliminary studies have shown that there are two distinct bands in the TPA spectrum that appear in the readily accessible wavelength region of $\sim 500 - 800$ nm, with corresponding one-photon transitions in the range $\sim 250 - 400$ nm.³⁵ Clearly, the ability to spectrally resolve two distinct bands will be an asset in examining potentially subtle solvent effects. Moreover, these harmine derivatives are soluble in polar protic (*e.g.* water) and polar aprotic (*e.g.* acetonitrile) solvents, both of which are readily tractable with molecular mechanics based computational methods (*i.e.*, force fields are available). For a realistic description of the environmental effects on the excited electronic states of the harmines, we employ the polarizable embedding (PE) model in combination with both TDDFT^{36,37} and CC response theory.^{38,39} In the PE model, the solvent molecules are represented by a detailed electrostatic and polarizable embedding potential consisting of higher-order distributed electric multipole moments, as well as anisotropic

electric dipole–dipole polarizabilities. This method not only accounts for the mutual polarization between the solvent and the solute in its ground electronic state, but it also incorporates the environmental response to the change in the electronic density of the solute upon excitation.

We report herein that distinct solvent effects are indeed observed in both one- and two-photon spectra of these chlorinated harmines. Moreover, we are able to model these solvent effects using the PE method in combination with TDDFT and CC response theory.

2 Experimental and computational details

2.1 Experiments

Preparation of samples. 6-Chloroharmine, 8-chloroharmine, 6,8-dichloroharmine⁴⁰ and 2,5-dibromo-1,4-bis(2-(4-(diphenylamino)phenyl)vinyl)benzene⁴¹ were synthesized according to procedures described in the references. All other chemicals and solvents (spectroscopic grade) were obtained from Sigma Aldrich and used as received.

In aqueous solution (milliQ water), the pH was adjusted to ~ 4 and to ~ 11 by adding drops of HCl and NaOH solutions, respectively. In acetonitrile, MeCN, the pH was adjusted to ~ 4 by adding drops of tri-fluoroacetic acid.

One-photon experiments. OPA spectra were recorded using 1 cm path length quartz cuvettes on a Shimadzu UV-3600 spectrometer.

Steady-state fluorescence measurements were performed using a Horiba Jobin Yvon spectrofluorometer. Corrected fluorescence spectra were recorded in a 1 cm path length quartz cell at room temperature. Fluorescence quantum yields were determined from the corrected fluorescence spectra, integrated over the entire emission profile. The standard used was quinine sulfate at pH 4 ($\Phi_f = 0.52 \pm 0.02$).⁴² To avoid inner filter effects, the absorbance of the solutions at the excitation wavelength was kept below 0.10.

Two-photon experiments. Two-photon excitation spectra and TPA cross-sections, σ^{TPA} , were determined upon irradiation with a fs laser system using the sample fluorescence as the

spectroscopic probe. Details of the experimental approach and instruments used have been published elsewhere.^{12,21} Briefly, a train of fs laser pulses was generated in a Ti:sapphire oscillator (Tsunami, Spectra Physics) and amplified using a regenerative amplifier (Spitfire, Spectra Physics). The output was either used directly (tunable from 780 to 840 nm) or down-converted in an optical parametric amplifier (OPA-800CF, Spectra Physics), resulting in pulses of approximately 130 fs FWHM and 15 nm spectral width. To cover the spectral range 560 – 760 nm, the second harmonic of the signal beam was employed. Appropriate long-pass filters were used to spectrally clean the laser output. The laser power was controlled using a half wave plate and a Glan-Taylor polarizer combined with neutral density filters. The laser beam was focused onto the sample by a $f = 500$ mm plano-convex lens. The fluorescence signal from two-photon excitations was spectrally isolated using appropriate interference filters and subsequently collected on a liquid nitrogen-cooled VIS/near-IR photomultiplier tube, PMT (Hamamatsu R5509-42). The output from the PMT was amplified and sent to (a) a photon counter (Stanford Research Systems model SR400) operated using a program written in LabView (National Instruments Inc.), or (b) a multiscaler photon counter (MSA300, Becker-Hickl).

TPA cross-sections were quantified against the following reference standards: 2,5-dibromo-1,4-bis(2-(4-(diphenylamino)phenyl)vinyl)benzene in toluene over the range 700 – 780 nm,^{12,21} 1,4-bis(2-methylstyryl)benzene in cyclohexane over the range 580 – 680 nm^{43,44} and fluorescein in aqueous solution at pH ~ 11 over the range 610 – 740 nm.¹³ All values were scaled to the fluorescein data at wavelengths where the respective data overlapped. The concentrations of the standards and harmine derivatives used range from 3 to 250 μM .

To yield a two-photon spectrum, excitation was performed at different wavelengths, and wavelength-dependent values of σ^{TPA} were quantified according to the formula¹¹

$$\sigma_S^{\text{TPA}} = \sigma_R^{\text{TPA}} \cdot \frac{I_S \cdot \Phi_{f,R} \cdot \eta_R \cdot P_R^2 \cdot C_R}{I_R \cdot \Phi_{f,S} \cdot \eta_S \cdot P_S^2 \cdot C_S}, \quad (1)$$

where the subscripts S and R refer to the sample and the reference, respectively. I is the collected fluorescence intensity and Φ_f is the fluorescence quantum yield (both under air-saturated conditions). P is the incident laser power and C is the solute concentration. Finally, η is a parameter that reflects the relative collection efficiency of the fluorescence, as calculated from the spectral overlap of the interference filters used, the fluorescence spectrum and the quantum efficiency of the PMT, with corrections for the refractive index of the solvent.

At each excitation wavelength, a power dependence study was performed to ensure that the transition was a true two-photon transition, *i.e.* ascertaining that the intensity of the fluorescence monitored increased quadratically with an increase in

the incident laser power. Specifically, at each excitation wavelength, the observed fluorescence intensity was plotted against the incident laser power on a double logarithmic plot for 4 to 7 data points. A slope of 2 is characteristic of two-photon excitation. Typically, slopes of 2.00 ± 0.05 were observed. However, under conditions of very low signal due to low TPA cross-sections, slopes of 2.00 ± 0.09 were accepted.

For a given harmine derivative, two-photon measurements were always performed for both solvents (H_2O and MeCN) in sequence to ensure that the measurements at each excitation wavelength were performed under identical experimental conditions. In this way we minimized the relative error on σ^{TPA} between the two solvents due to any drift of the experimental conditions. Two-photon experiments were likewise performed using 1 cm path length cuvettes.

2.2 Computational procedure

Classical molecular dynamics (MD) simulations of the three solvated harmines in the two solvents (H_2O and MeCN) were performed to produce 100 snapshots per simulation, see Supplementary Information (SI) for details. To refine the internal solute molecular geometries with respect to those obtained using classical force fields, the solute-solvent configurations used in the subsequent PE property calculations were generated by a point-charge electrostatic quantum mechanics/molecular mechanics (QM/MM) geometry optimization of the solute, while keeping the solvent fixed to the MD configuration, using the Qsite program.⁴⁵ By this, a part of the temperature effects is lost. On the other hand, we secure a high level solute structure quality, which is very important for reliable property calculations.

The solvent embedding potentials needed for the OPA and TPA calculations of the solute-solvent systems consisted of atom-distributed electric multipole moments up to and including quadrupoles, as well as anisotropic electric dipole-dipole polarizabilities (referred to as M2P2 embedding potential), as obtained according to the LoProp⁴⁶ approach implemented in the Molcas program.^{47,48} The generation of the embedding potentials was facilitated by the PE Assistant Script (PEAS).⁴⁹

The OPA properties of the two lowest excited singlet states of the three harmines in water and acetonitrile, respectively, were independently calculated with (a) PE-TDDFT^{36,37} using the CAM-B3LYP⁵⁰ exchange-correlation functional, and (b) PERI-CC2.³⁸ Two-photon cross sections have been implemented for RI-CC2,⁵¹ but an analogous PE version has not been published yet. The TPA properties were therefore calculated only with the PE-TDDFT method. The aug-cc-pVDZ basis set⁵² was applied in all cases. The PE-TDDFT calculations were calculated using the Dalton quantum chemistry program,^{53,54} whereas the PERI-CC2 calculations were performed using the Turbomole program package.⁵⁵ These

calculations resulted in a set of excitation energies, oscillator strengths and TPA probabilities for the two lowest excited states of each snapshot. The illustrations of the time-development of these values are given in Figure S1 in the SI.

Spectral broadening due to quantized vibrations was not explicitly included although it is potentially important.⁵⁶ To generate computed OPA and TPA spectra comparable with their experimental counterparts, a constant spectral width was assigned by convoluting each transition with a Lorentzian distribution function. The broadening that simulates the fine structure of the spectrum was regulated according to the experimentally-observed full width at half maximum (FWHM); *i.e.*, the Lorentzian distribution was chosen so that the FWHM of the computed spectra (0.35 eV for OPA spectra and 0.2 eV for TPA spectra) best resemble the FWHM of the experimental spectra. The absolute values of molar absorption coefficients (ϵ) and two-photon absorption cross sections (σ^{TPA}) were calculated from oscillator strengths and two-photon absorption probabilities, respectively. The details of the procedures are given in the SI.

The vacuum geometries of the three protonated harmine derivatives were optimized using the Turbomole package at the B3LYP/TZP level of theory and their OPA and TPA properties were calculated in the same manner as for the solution calculations.

3 Results

3.1 Experimental results

The experimental OPA spectra for the 3 harmine derivatives are shown in Figure 2. Selected photophysical properties are collected in Table 1.

In general, for all the harmine derivatives studied, a blue shift of a few nanometers in the absorption maximum together with a decrease of the molar absorption coefficient is observed when changing the solvent from MeCN to H₂O. The feature is most pronounced for 8-chloroharmine. 8-Chloroharmine is also unique in that it does not clearly show the two distinct absorption bands seen in the 6-chloro and 6,8-dichloro derivatives. Although there appears to be a systematic increase in the fluorescence quantum yield of these three compounds as the solvent is changed from MeCN to H₂O, these changes do not exceed the margins of error from our experiment.

Two photon excitation spectra are shown in Figure 3 and TPA cross-sections are given in Table 2. As for the one-photon data, there appears to be a general blue shift in the band maximum together with a clear decrease of the two-photon cross-section when changing the solvent from MeCN to H₂O. It should be noted, however, that the actual blue shift is hard to quantify due to the limited spectral resolution available with the fs laser pulses used for excitation.

Furthermore, the two-photon spectra of all three harmine derivatives resemble the respective one-photon absorption spectra recorded at half the wavelength. This indicates that the electronic states populated in the two-photon process are the same as those populated upon one-photon excitation at half the wavelength. This agrees with the fact that all three molecules lack an inversion center^{21,57,58} and all excited states are symmetry allowed for both one- and two-photon absorption.

The two-photon cross-sections given in Table 2 have an estimated absolute accuracy that, at most, is $\pm 30\%$, which reflects the reported error in the standards ($\sim \pm 15\%$) combined with the error in our present measurements ($\sim \pm 15\%$), arising from uncertainties in sample concentrations, laser powers, etc., as embodied in Eq. (1). However the relative uncertainty for a given harmine derivative at each point in the spectrum is estimated to be significantly lower ($\pm 10\%$), and the relative error between the two solvents is estimated to be less than $\pm 15\%$.

3.2 Computational results

The first noticeable feature of both one- and two-photon computed spectra is their remarkable resemblance in shape with the respective experimental spectra (Figures 2 and 3). In all cases, the harmine derivatives have weaker OPA and TPA bands in H₂O than in MeCN. It is also apparent that all the bands for H₂O solutions are slightly blue-shifted with respect to those in the MeCN solutions. The difference is more pronounced for the second excited state because of the more narrow line width. The computations also model the unique feature that the 6-chloro and 6,8-dichloro derivatives show two distinct bands whereas the corresponding bands are appreciably overlapped in the spectra of the 8-chloro derivative. Although the absolute magnitudes for the calculated one- and two-photon transition probabilities (*i.e.*, ϵ_{max} and σ^{TPA}) appear to differ slightly from the corresponding experimental values, these differences are negligible considering the errors involved. Pertinent parameters are listed in Tables 1 and 2.

When comparing the absolute positions of the bands, PERI-CC2 gives better agreement with the experiment than PE-TDDFT; the excitation energies are overestimated by 0.3 to 0.4 eV in the PERI-CC2 model, whereas PE-TDDFT overestimates the values by 0.5 to 0.6 eV. This is in line with the expectations that the CC method yields more accurate excitation energies than DFT.⁵⁹ On the other hand, the computations model the absolute magnitudes of the solvent-dependent blue shifts in the band maxima quite well. To obtain higher accuracy than 0.3 eV in comparison with experiment, it would be necessary to include the contributions from molecular vibrations to zero-point energies and spectral profiles, as well as more accurate CC models including triples excitations.

In contrast, as seen from the OPA calculations (Table 1), the PE-TDDFT and PERI-CC2 methods yield similar values

Table 1 Selected one-photon experimental and computational photophysical properties of the studied harmine derivatives: wavelengths of band maxima (λ_{\max}), maximum molar absorption coefficients (ϵ_{\max}) and quantum yields of fluorescence (Φ_f) in water and acetonitrile.

	molecule	transition	$\lambda_{\max}^{\text{abs}}/\text{nm}$		$\epsilon_{\max}^{\dagger} \cdot 10^{-4}/\text{M}^{-1}\text{cm}^{-1}$		Φ_f	
			water	MeCN	water	MeCN	water	MeCN
experiment	6-Cl-Ha	$S_0 \rightarrow S_1$	362	367	0.902	1.020	0.16 ± 0.02	0.14 ± 0.02
		$S_0 \rightarrow S_2$	317	321	2.406	2.590		
	8-Cl-Ha	$S_0 \rightarrow S_1$	-	-	-	-	0.11 ± 0.02	0.09 ± 0.02
		$S_0 \rightarrow S_2$	321	327	1.672	1.904		
	6,8-diCl-Ha	$S_0 \rightarrow S_1$	369	369	0.633	0.689	0.20 ± 0.02	0.17 ± 0.02
		$S_0 \rightarrow S_2$	305	308	1.890	2.102		
	molecule	transition	λ_{\max}/nm		$\epsilon_{\max} \cdot 10^{-4}/\text{M}^{-1}\text{cm}^{-1}$		$\lambda_{\text{excit}}/\text{nm}$ vacuum	$\epsilon \cdot 10^{-4}/\text{M}^{-1}\text{cm}^{-1}$ vacuum
			water	MeCN	water	MeCN		
(PE)RI-CC2 [§]	6-Cl-Ha	$S_0 \rightarrow S_1$	328	332	0.794	0.935	367	0.859
		$S_0 \rightarrow S_2$	289	294	1.851	1.956	342	2.060
	8-Cl-Ha	$S_0 \rightarrow S_1$	328 [‡]	328 [‡]	-	-	365	1.114
		$S_0 \rightarrow S_2$	295	300	1.686	1.998	345	1.536
	6,8-diCl-Ha	$S_0 \rightarrow S_1$	338	340	0.580	0.618	372	0.333
		$S_0 \rightarrow S_2$	277	281	1.477	1.700	346	2.235
	molecule	transition	λ_{\max}/nm		$\epsilon_{\max} \cdot 10^{-4}/\text{M}^{-1}\text{cm}^{-1}$		$\lambda_{\text{excit}}/\text{nm}$ vacuum	$\epsilon \cdot 10^{-4}/\text{M}^{-1}\text{cm}^{-1}$ vacuum
			water	MeCN	water	MeCN		
(PE-)TDDFT [§]	6-Cl-Ha	$S_0 \rightarrow S_1$	305	308	0.808	0.888	343	0.567
		$S_0 \rightarrow S_2$	278	281	1.805	2.010	317	2.184
	8-Cl-Ha	$S_0 \rightarrow S_1$	309 [‡]	309 [‡]	-	-	336	0.610
		$S_0 \rightarrow S_2$	281	284	1.813	2.063	319	1.916
	6,8-diCl-Ha	$S_0 \rightarrow S_1$	313	314	0.628	0.666	348	0.557
		$S_0 \rightarrow S_2$	271	273	1.418	1.619	318	3.670

[†] The error is ± 5 %. For the experimental data, we assume that the molar extinction coefficient accurately reflects the molar absorption coefficient.

[‡] These values are obtained by averaging the excitation energies of snapshots and not as the maximum of absorption as for the other states.

[§] No PE approach was applied in vacuum calculations.

for the transition probabilities (*i.e.* ϵ^{\max}).

4 Discussion

Interesting insight is provided by pictures of the molecular orbitals (MOs) involved in the transitions (Figure 4). The first excited state is predominantly composed of the transition from the highest occupied MO to the lowest unoccupied MO (HOMO → LUMO), while the second excited state corresponds to a transition from the second highest occupied MO to the LUMO (HOMO – 1 → LUMO). The charge distributions and changes in charge distribution, represented by the occupancy of these orbitals (*i.e.*, dipole moments and changes in dipole moments, respectively), also provide important insight with respect to the solvent effects observed on the spectra.

Table 3 reports the calculated dipole moments of the pertinent ground and excited states. While the absolute size of the dipole moment of a charged molecule depends on the choice of origin of the coordinate system, the change in dipole moments upon excitation does not. In all cases, dipole moments decrease appreciably upon excitation. This is consistent with the orbital picture as well, where HOMO – 1 and HOMO have a significant amount of electron density on the chlorine atoms, whereas the LUMO orbital has very little electron density on chlorine atoms (no density is seen for the given isocontour value). In other words, upon excitation, the electron density (negative charge) moves towards the more positively charged region of the molecule. On this basis, the ground state would be more stabilized than the excited state in a polar solvent and the energy gap between the two states would increase. Thus,

Table 2 Experimental and PE-TDDFT TPA cross-sections of the studied harmine derivatives.

molecule	transition	experiment				PE-TDDFT			
		$\lambda_{\text{max}}^{\text{TPA}} / \text{nm}$		$\sigma^{\text{TPA}} / \text{GM}$		$\lambda_{\text{max}}^{\text{TPA}} / \text{nm}$		$\sigma^{\text{TPA}} / \text{GM}$	
		water	MeCN	water	MeCN	water	MeCN	water	MeCN
6-Cl-Ha	$S_0 \rightarrow S_1$	730	730	3.7 ± 0.8	5.4 ± 1.1	621	629	1.73	2.26
	$S_0 \rightarrow S_2$	640	640	6.6 ± 1.4	8.5 ± 1.8	560	565	8.21	10.4
8-Cl-Ha	$S_0 \rightarrow S_1$	-	-	-	-	618 [†]	620 [†]	-	-
	$S_0 \rightarrow S_2$	620	660	5.4 ± 1.4	7.4 ± 2.1	566	571	7.86	10.9
6,8-diCl-Ha	$S_0 \rightarrow S_1$	730	730	1.1 ± 0.2	1.6 ± 0.3	637	638	0.565	0.684
	$S_0 \rightarrow S_2$	600	620	3.5 ± 0.7	5.1 ± 1.1	546	549	4.84	6.40

[†] These values are obtained by averaging the excitation energies of snapshots and not as the maximum of absorption as for the other cases.

Table 3 Dipole moments[†] of ground (S_0) and first two excited states (S_1 , S_2), as well as changes in dipole moments upon excitation in vacuum (RI-CC2/aug-cc-pVDZ and CAM-B3LYP/aug-cc-pVDZ, in Debye).

	molecule	$\mu(S_0)$	$\mu(S_1)$	$\mu(S_2)$	$\Delta\mu(S_0 \rightarrow S_1)$	$\Delta\mu(S_0 \rightarrow S_2)$
RI-CC2	6-Cl-Ha	13.43	6.08	5.71	- 7.35	- 7.72
	8-Cl-Ha	10.87	0.84	3.78	- 10.03	- 7.09
	6,8-diCl-Ha	14.19	6.48	3.56	- 7.71	- 10.63
TDDFT	6-Cl-Ha	12.14	6.82	8.36	- 5.32	- 3.78
	8-Cl-Ha	9.22	3.42	4.73	- 5.80	- 4.49
	6,8-diCl-Ha	13.36	7.76	8.87	- 5.50	- 4.49

[†] For all molecules, the center of mass is used as the coordinate origin. While the absolute values of the dipole moment of a charged molecule depend on the position of the origin of the coordinate system, the change in the dipole moment can be obtained independently of this origin.

absorption bands recorded in a polar solvent would be blue-shifted relative to bands recorded in a gas-phase experiment. This is indeed seen in Table 1, where calculations in H₂O and MeCN show spectral blue shifts of about 30 to 50 nm, respectively, compared to the corresponding transition for an isolated gas-phase molecule. Carrying this point further, the dielectric constant of H₂O is around 80 and of MeCN is around 38. This means that the ground state would be more stabilized in H₂O than in MeCN. This is consistent with the observation that the bands recorded when using H₂O as the solvent are slightly blue-shifted relative to the bands recorded from MeCN solutions.

The characteristic spectral profile of 8-chloroharmine relative to the 6-chloro and 6,8-dichloro derivatives (*i.e.*, two overlapped bands vs. two well-defined bands) also appears to be consistent with the fact that the first excited state of the 8-chloro derivative has a comparatively small dipole moment (Table 3). This state in the 8-chloro derivative is thus less stabilized in a polar solvent and comes closer to the energy of the

second excited state, and it appears more as a shoulder than as a distinct band.

An important aspect of our study is that these solutes will also interact with solvent molecules via hydrogen bonds, with H₂O arguably being more important than MeCN in this regard. An analysis of hydrogen bonding using the QM/MM optimized structures shows that there are generally three sites on these chromophores that participate in hydrogen bonds (Figure 5). These are the two hydrogen donating N-H groups and the hydrogen accepting oxygen atom on the methoxy group. The H₂O-solvated chromophores generally form between one and three hydrogen bonds, whereas the MeCN-solvated chromophores usually form no or one hydrogen bond. To estimate the effect of hydrogen bonding on the absorption spectra, compared to the overall effect of the polarizable environment, pertinent spectroscopic parameters for the hydrogen-bonded molecular clusters shown in Figure 5 have been calculated with the PE-TDDFT description under a variety of conditions. These clusters were chosen from available MD snapshots, so

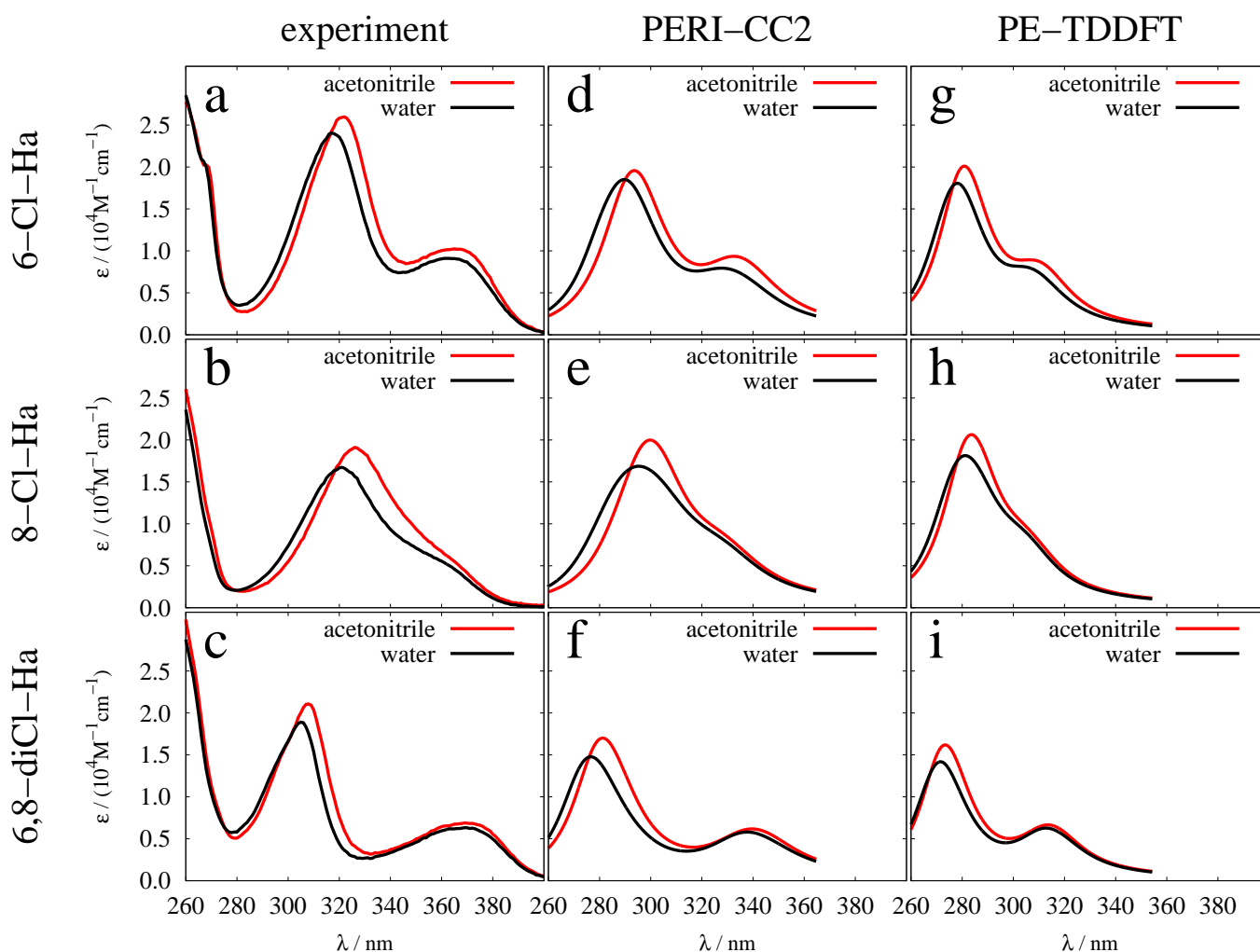


Fig. 2 Matrix showing the comparison of OPA spectra of 6-Cl-Ha (a, d, g), 8-Cl-Ha (b, e, h) and 6,8-diCl-Ha (c, f, i) obtained from experiment (a-c), with PERI-CC2 (d-f) and with PE-DFT (g-i).

that all the sites prone to hydrogen bonding are occupied. It is hard to predict the number of hydrogen bonds that would yield the largest effect on the OPA and the TPA spectra, but a snapshot with the highest number of hydrogen bonds was chosen for further studies. The results are shown in Table 4. M2P0 refers to the use of an embedding potential corresponding to turning off polarization in the PE potential (in contrast to M2P2 which includes this explicit polarization). Note that there are two vacuum results, because the geometries are not vacuum-optimized, but come from two different MD simulations and are QM/MM-optimized in the presence of their respective solvent. It is clear that the effect of hydrogen bonding is manifested on both excitation energies and two-photon transition probabilities. As discussed above, the latter arises from the fact that the transition probability depends on the change

in the dipole moments, which is likewise affected by the hydrogen bonding. In fact, the PE method gives an excellent description of the interaction of a chromophore with its nearest surrounding through hydrogen bonding, (*i.e.* Table 4 shows that the full QM description of the hydrogen bonded cluster of chromophore with solvent molecules gives only marginal improvement over the PE description of the same region). This is important since inclusion of further solvent molecules in the QM region rapidly becomes a challenging computational problem, while the computational cost of including 2 or 200 solvent molecules in the PE description is relatively similar. It is also beneficial to include polarization effects when one calculates non-linear optical properties. This improvement in description of solvent-solute interactions goes with little additional computational cost.

Table 4 Comparison of excitation energies (ω), OPA oscillator strengths (f) and two-photon transition strengths (δ^{TPA}) of the first two excited states of a molecule of 6,8-dichloroharmine in vacuum (two different geometries), surrounded with a maximum number of hydrogen bonded non-polarizable (N M2P0 x) and polarizable (N M2P2 x) solvent molecules, surrounded with a maximum number of quantum-mechanically described hydrogen bonded solvent molecules (N QM x), in the entire polarizable solvent box (full M2P2 x) and in the entire polarizable solvent box with QM description of hydrogen bonded solvent molecules (N QM x + full M2P2 x). Here N denotes the number of hydrogen bonded solvent molecules and x is solvent molecule (H_2O or MeCN). Computational model is (PE-)CAM-B3LYP/aug-cc-pVDZ.

	environment	ω_1/eV	f_1	$\delta_1^{\text{TPA}}/\text{a.u.}$	ω_2/eV	f_2	$\delta_2^{\text{TPA}}/\text{a.u.}$
water	vacuum	3.523	0.0647	250	4.072	0.3272	2652
	3 M2P0 H_2O	3.560	0.0665	177	4.200	0.2848	1889
	3 M2P2 H_2O	3.573	0.0874	177	4.229	0.2834	1812
	3 QM H_2O	3.571	0.0699	200	4.217	0.2932	1933
	full M2P0 H_2O	3.858	0.0921	124	4.527	0.2685	902
	full M2P2 H_2O	3.898	0.1147	98	4.607	0.3011	801
	3 QM H_2O + full M2P2 H_2O	3.895	0.1160	113	4.598	0.3138	865
	vacuum	3.562	0.08882	582	4.014	0.3571	2862
acetonitrile	2 M2P0 MeCN	3.652	0.0910	450	4.147	0.3141	2189
	2 M2P2 MeCN	3.679	0.0928	417	4.190	0.3596	2059
	2 QM MeCN	3.672	0.0932	437	4.183	0.3299	2088
	full M2P0 MeCN	3.934	0.0932	132	4.430	0.2920	1114
	full M2P2 MeCN	3.909	0.1151	173	4.414	0.3601	1505
	2 QM MeCN + full M2P2 MeCN	3.902	0.1172	188	4.408	0.3773	1550

The computational results in Table 4 also show some interesting trends between the excitation energy of a given transition and the probability of the transition: the OPA oscillator strength tends to increase with an increase in the excitation energy, whereas the TPA cross section tends to decrease (*i.e.* a negative correlation). Although the results of our response calculations in this regard are not readily interpreted in the context of the more traditional sum-over-states (SOS) model,^{61–63} we can nevertheless evaluate how these parameters evolve for each of the 100 snapshots used in our calculations (see SI). In the least, there indeed appears to be a clear negative correlation between the excitation energy and the TPA cross section. The negative dependency of the TPA transition probabilities on excitation energies are also consistent with the observations that the H_2O -solvated chromophores absorb less intensively than the MeCN-solvated, while their band maxima are blue shifted with respect to the band maxima in MeCN solutions.

5 Conclusion

We have performed a combined experimental and computational study of the OPA and TPA spectra of three chlorinated harmine in two different solvents. These molecular systems were chosen because they are large enough to facilitate exper-

imental work but small enough to be treated with reasonably high level computational methods.

We show that information-rich, solvent-dependent spectra can indeed be accurately modeled using computations. Specifically, our computational procedure was able to reproduce subtle solvent-dependent spectral shifts and changes in both one- and two-photon transition probabilities. The computations systematically overestimated the experimentally observed transition energies, by ~ 0.3 eV for PERI-CC2 and ~ 0.6 eV for PE-TDDFT.

High accuracy methods like CC3 are needed to systematically approach the experimental excitation energies, as is also inclusion of vibrational effects, instead of only vertical excitations. A more accurate classical force field used in MD simulations, which could yield a better description of finite temperature effects and solvent geometries is also important.

The promising results of the PERI-CC2 model indicate the need to further develop *ab initio* methods for modeling TPA processes in the PE context. A successful implementation of PERI-CC2 for TPA would give broader possibilities for better descriptions of photoactive systems like proteins, where environment can play a crucial role in the enhancement of spectroscopic properties of chromophores.

6 Acknowledgements

This work was supported by a grant from the Danish National Research Foundation. D.H. acknowledges funding from The Marie Curie ITN, Grant Agreement 2010-264362. O.C. acknowledges support from the Lundbeck Foundation, the Danish e-Infrastructure Cooperation (DeIC), and the Danish Council for Independent Research through a Sapere Aude III grant (DFF – 4002-00015). J.K. acknowledges the Lundbeck and Villum Foundations, DeIC, and the Danish Council for Independent Research (the Sapere Aude programme) for financial support. This work was also supported by ANPCyT (PICT 20120423 and 20132536), Argentina. M.P.D., R.E.-B., and F.M.C. are research members of CONICET (Argentina).

References

- M. Pawlicki, H. Collins, R. Denning and H. Anderson, *Angew. Chem. Int. Ed.*, 2009, **48**, 3244–3266.
- F. Terenziani, C. Katan, E. Badaeva, S. Tretiak and M. Blanchard-Desce, *Adv. Mat.*, 2008, **20**, 4641–4678.
- W. Denk, J. Strickler and W. Webb, *Science*, 1990, **248**, 73–76.
- K. König, P. T. C. So, W. W. Mantulin, B. J. Tromberg and E. Gratton, *J. Microsc.*, 1996, **183**, 197–204.
- F. Stellacci, C. Bauer, T. Meyer-Friedrichsen, W. Wenseleers, V. Alain, S. Kuebler, S. Pond, Y. Zhang, S. Marder and J. Perry, *Adv. Mat.*, 2002, **14**, 194–198.
- B. Hudson and B. Kohler, *Chem. Phys. Lett.*, 1972, **14**, 299–304.
- R. R. Birge, *Acc. Chem. Res.*, 1986, **19**, 138–146.
- W. M. McClain, *J. Chem. Phys.*, 1971, **55**, 2789–2796.
- P. R. Ogilby, *Chem. Soc. Rev.*, 2010, **39**, 3181–3209.
- M. Albota, D. Beljonne, J.-L. Brédas, J. E. Ehrlich, J.-Y. Fu, A. A. Heikal, S. E. Hess, T. Kogej, M. D. Levin, S. R. Marder, D. McCord-Maughon, J. W. Perry, H. Röckel, M. Rumi, G. Subramaniam, W. W. Webb, X.-L. Wu and C. Xu, *Science*, 1998, **281**, 1653–1656.
- C. Xu and W. W. Webb, *J. Opt. Soc. Am. B*, 1996, **13**, 481–491.
- J. Arnbjerg, M. Johnsen, P. K. Frederiksen, S. E. Braslavsky and P. R. Ogilby, *J. Phys. Chem. A*, 2006, **110**, 7375–7385.
- N. S. Makarov, M. Drobizhev and A. Rebane, *Opt. Express*, 2008, **16**, 4029–4047.
- N. H. List, F. M. Pimenta, L. Holmegaard, R. L. Jensen, M. Etzerodt, T. Schwabe, J. Kongsted, P. R. Ogilby and O. Christiansen, *Phys. Chem. Chem. Phys.*, 2014, **16**, 9950–9959.
- M. Drobizhev, S. Tillo, N. S. Makarov, T. E. Hughes and A. Rebane, *J. Phys. Chem. B*, 2009, **113**, 855–859.
- M. Kruk, A. Karotki, M. Drobizhev, V. Kuzmitsky, V. Gael and A. Rebane, *JOL*, 2003, **105**, 45–55.
- N. A. Murugan, J. Kongsted, Z. Rinkevicius, K. Aidas, K. V. Mikkelsen and H. Ågren, *Phys. Chem. Chem. Phys.*, 2011, **13**, 12506–12516.
- M. Wielgus, R. Zalesny, N. A. Murugan, J. Kongsted, H. Ågren, M. Samoc and W. Bartkowiak, *ChemPhysChem*, 2013, **14**, 3731–3739.
- N. S. Makarov, S. Mukhopadhyay, K. Yesudas, J.-L. Brédas, J. W. Perry, A. Pron, M. Kivala and K. Müllen, *J. Phys. Chem. A*, 2012, **116**, 3781–3793.
- I. Fedorov, L. Koziol, A. K. Mollner, A. I. Krylov and H. Reisler, *J. Phys. Chem. A*, 2009, **113**, 7412–7421.
- J. Arnbjerg, M. J. Paterson, C. B. Nielsen, M. Jørgensen, O. Christiansen and P. R. Ogilby, *J. Phys. Chem. A*, 2007, **111**, 5756–5767.
- J. Olsen and P. Jørgensen, *J. Chem. Phys.*, 1985, **82**, 3235–3264.
- O. Christiansen, P. Jørgensen and C. Hättig, *Int. J. Quant. Chem.*, 1998, **68**, 1–52.
- E. Runge and E. K. U. Gross, *Phys. Rev. Lett.*, 1984, **52**, 997–1000.
- M. Johnsen and P. R. Ogilby, *J. Phys. Chem. A*, 2008, **112**, 7831–7839.
- H. Woo, J. Hong, B. Liu, A. Mikhailovsky, D. Korystov and G. Bazan, *J. Am. Chem. Soc.*, 2005, **127**, 820–821.
- M. Wielgus, W. Bartkowiak and M. Samoc, *Chem. Phys. Lett.*, 2012, **554**, 113–116.
- M. Wielgus, J. Michalska, M. Samoc and W. Bartkowiak, *Dyes Pigments*, 2015, **113**, 426–434.
- G. Wicks, A. Rebane and M. Drobizhev, *Proc. SPIE*, 2014, **8983**, 89830R–89830R–11.
- N. B. Neto, D. Correa, L. D. Boni, G. Parra, L. Misoguti, C. Mendonça, I. Borissevitch, S. Zílio and P. Gonçalves, *Chem. Phys. Lett.*, 2013, **587**, 118–123.
- F. Terenziani, A. Painelli, C. Katan, M. Charlot and M. Blanchard-Desce, *J. Am. Chem. Soc.*, 2006, **128**, 15742–15755.
- A. Blázquez-Castro, T. Breitenbach and P. R. Ogilby, *Photochem. Photobiol. Sci.*, 2014, **13**, 1235–1240.
- F. Lamchouri, A. Settaf, Y. Cherrah, M. Hassar, M. Zemzami, N. Atif, E. Nadori, A. Zaid and B. Lyoussi, *Fitoterapia*, 2000, **71**, 50–54.
- S. S. H. Tehrani, S. H. S. Shabani, S. T. Enferadi and Z. Rabiei, *Iran. J. Biotech.*, 2014, **12**, e18562.
- M. M. Gonzalez, J. Arnbjerg, M. P. Denofrio, R. Erra-Balsells, P. R. Ogilby and F. M. Cabrerizo, *J. Phys. Chem. A*, 2009, **113**, 6648–6656.
- J. M. H. Olsen and J. Kongsted, *Advances in Quantum Chemistry*, 2011, **61**, 107–143.
- J. M. H. Olsen, K. Aidas and J. Kongsted, *J. Chem. Theory Comput.*, 2010, **6**, 3721–3734.
- T. Schwabe, K. Sneskov, J. M. H. Olsen, J. Kongsted, O. Christiansen and C. Hättig, *J. Chem. Theory Comput.*, 2012, **8**, 3274–3283.
- K. Sneskov, T. Schwabe, J. Kongsted and O. Christiansen, *J. Chem. Phys.*, 2011, **134**, year.
- M. A. Ponce, O. I. Tarzi and R. Erra-Balsells, *J. Heterocyclic Chem.*, 2003, **40**, 419–426.
- P. K. Frederiksen, M. Jørgensen and P. R. Ogilby, *J. Am. Chem. Soc.*, 2001, **123**, 1215–1221.
- S. R. Meech and D. Phillips, *J. Photochem.*, 1983, **23**, 193–217.
- S. M. Kennedy and F. E. Lytle, *Anal. Chem.*, 1986, **58**, 2643–2647.
- W. G. Fisher, E. A. Wachter, F. E. Lytle, M. Armas and C. Seaton, *Appl. Spectrosc.*, 1998, **52**, 536–545.
- QSite, version 5.8, Schrödinger, LLC, New York, NY*, Schrödinger, LLC, New York, NY, 2012.
- L. Gagliardi, R. Lindh and G. Karlström, *J. Chem. Phys.*, 2004, **121**, 4494–4500.
- G. Karlström, R. Lindh, P.-Å. Malmqvist, B. O. Roos, U. Ryde, V. Veryazov, P.-O. Widmark, M. Cossi, B. Schimmelpfennig, P. Neogrady and L. Seijo, *Comput. Mater. Sci.*, 2003, **28**, 222–239.
- F. Aquilante, L. De Vico, N. Ferré, G. Ghigo, P.-Å. Malmqvist, P. Neogrady, T. B. Pedersen, M. Pitoňák, M. Reiher, B. O. Roos, L. Serrano-Andrés, M. Urban, V. Veryazov and R. Lindh, *J. Comput. Chem.*, 2010, **31**, 224–247.
- J. M. H. Olsen, *PhD thesis*, University of Southern Denmark, Odense, Denmark, 2012.
- T. Yanai, D. P. Tew and N. C. Handy, *Chem. Phys. Lett.*, 2004, **393**, 51–57.
- D. H. Friese, C. Hättig and K. Ruud, *Phys. Chem. Chem. Phys.*, 2012, **14**, 1175–1184.
- T. H. Dunning, *J. Chem. Phys.*, 1989, **90**, 1007–1023.
- DALTON, a molecular electronic structure program, Release Dalton2011, see <http://daltonprogram.org/>*, 2011.
- K. Aidas, C. Angeli, K. L. Bak, V. Bakken, R. Bast, L. Boman, O. Christiansen, R. Cimирaglia, S. Coriani, P. Dahle, E. K. Dalskov, U. Ekström, T. Enevoldsen, J. J. Eriksen, P. Eitenhuber, B. Fernández, L. Ferrighi, H. Fliegl, L. Frediani, K. Hald, A. Halkier, C. Hättig, H. Heiberg, T. Hel-

- gaker, A. C. Hennum, H. Hettema, E. Hjertenæs, S. Høst, I.-M. Høyvik, M. F. Iozzi, B. Jansik, H. J. A. Jensen, D. Jonsson, P. Jørgensen, J. Kauczor, S. Kirpekar, T. Kjærgaard, W. Klopper, S. Knecht, R. Kobayashi, H. Koch, J. Kongsted, A. Krapp, K. Kristensen, A. Ligabue, O. B. Lutnæs, J. I. Melo, K. V. Mikkelsen, R. H. Myhre, C. Neiss, C. B. Nielsen, P. Norman, J. Olsen, J. M. H. Olsen, A. Osted, M. J. Packer, F. Pawłowski, T. B. Pedersen, P. F. Provasi, S. Reine, Z. Rinkevičius, T. A. Ruden, K. Ruud, V. V. Rybkin, P. Sałek, C. C. M. Samson, A. S. de Merás, T. Saue, S. P. A. Sauer, B. Schimmelpfennig, K. Sneskov, A. H. Steindal, K. O. Sylvester-Hvid, P. R. Taylor, A. M. Teale, E. I. Tellgren, D. P. Tew, A. J. Thorvaldsen, L. Thøgersen, O. Vahtras, M. A. Watson, D. J. D. Wilson, M. Ziolkowski and H. Ågren, *Wiley Interdisciplinary Reviews: Computational Molecular Science*, 2014, **4**, 269–284.
- 55 *TURBOMOLE V6.4 2012, a development of University of Karlsruhe and Forschungszentrum Karlsruhe GmbH, 1989-2007, TURBOMOLE GmbH, since 2007; available from <http://www.turbomole.com>.*
- 56 N. Lin, Y. Luo, K. Ruud, X. Zhao, F. Santoro and A. Rizzo, *ChemPhysChem*, 2011, **12**, 3392–3403.
- 57 W. M. McClain, *Acc. Chem. Res.*, 1974, **7**, 129–135.
- 58 C. B. Nielsen, J. Arnbjerg, M. Johnsen, M. Jørgensen and P. R. Ogilby, *J. Org. Chem.*, 2009, **74**, 9094–9104.
- 59 N. H. List, J. M. H. Olsen, T. Rocha-Rinza, O. Christiansen and J. Kongsted, *Int. J. Quant. Chem.*, 2012, **112**, 789–800.
- 60 G. Schaftenaar and J. Noordik, *J. Comput.-Aided Mol. Design*, 2000, **14**, 123–134.
- 61 B. Orr and J. Ward, *Mol. Phys.*, 1971, **20**, 513–526.
- 62 R. R. Birge and B. M. Pierce, *J. Chem. Phys.*, 1979, **70**, 165–178.
- 63 B. Dick and G. Hohlneicher, *Theoret. chim. acta*, 1979, **53**, 221–251.

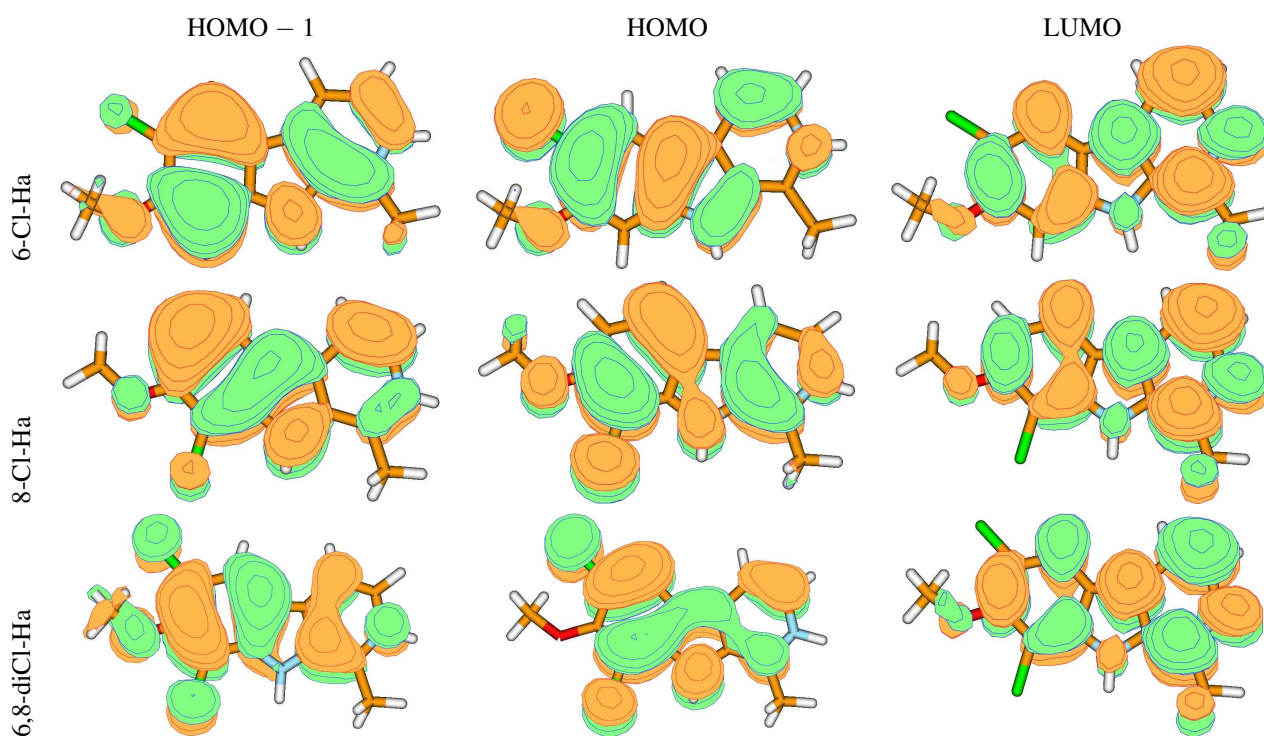


Fig. 4 Molecular orbitals that participate in the first two excited states (HF/aug-cc-pVDZ, contour value = 0.02 a.u.). Calculations were performed for molecules in the gas phase and the orientation of the molecules is the same as in Figure 1. The orbital plots are produced using the Molden 5.0 program.⁶⁰

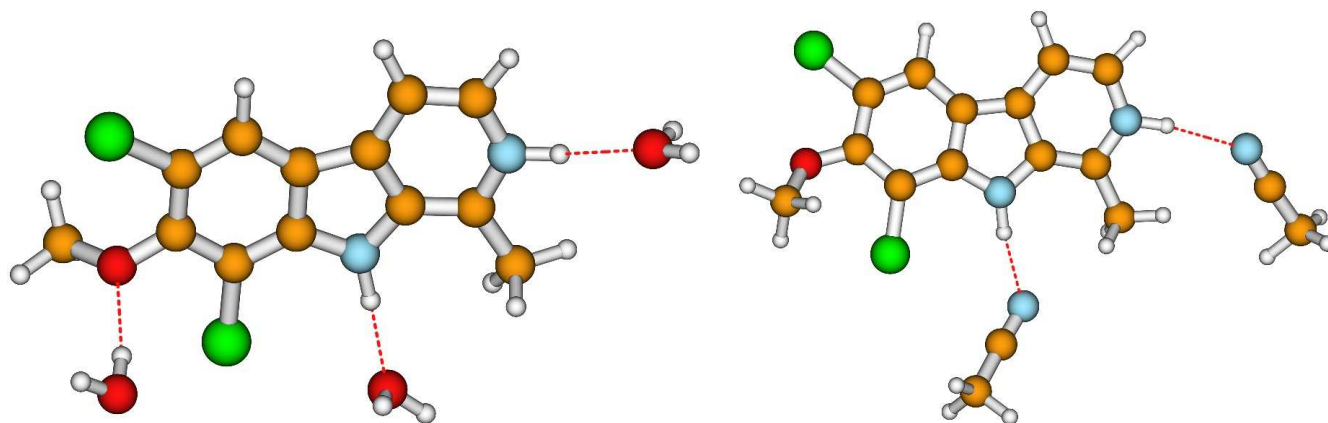


Fig. 5 6,8-dichloro-harmine molecule hydrogen bonded with 3 water molecules (left) and 2 acetonitrile molecules (right). The molecular plots are produced using the Molden 5.0 program.⁶⁰